Soft Matter

Accepted Manuscript

ROYAL SOCIETY OF CHEMISTRY

www.rsc.org/softmatter

Graphic abstract:

Facilely Determining Solubility of β-Nucleating Agent by Gradient Temperature Field for Construction of Heterogeneous Crystalline-Frameworks in iPP

Zhiqiang Wu[a], *Gang Wang*[a], *Mengwei Zhang*[a], *Ke Wang*[a,*], *and Qiang Fu*[a,*]

[a] College of Polymer Science and Engineering, Sichuan University, State Key Laboratory of Polymer Materials Engineering, Chengdu 610065, People's Republic of China

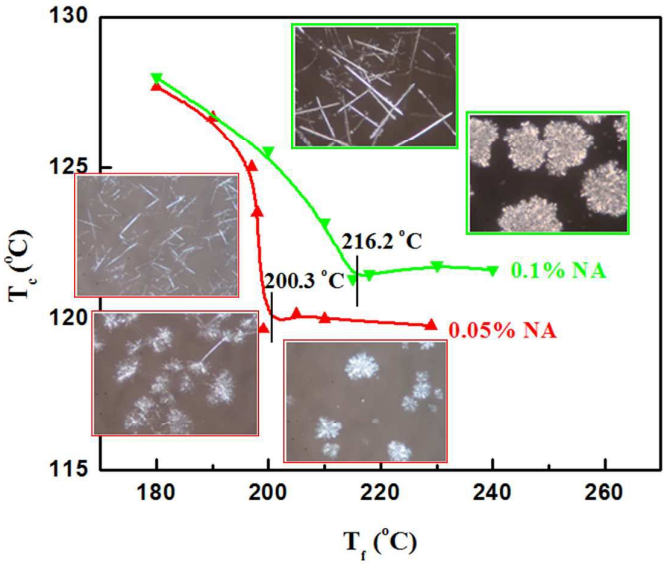

The transformation from "sensitive" to "insensitive" might be referred to completely dissolve NA.

Soft Matter

ARTICLE

Facilely Assess The Soluble Behaviour of β-Nucleating Agent by Gradient Temperature Field for Construction of Heterogeneous Crystalline-Frameworks in iPP

Received 00th January 20xx,
Accepted 00th January 20xx

DOI: 10.1039/x0xx00000x

www.rsc.org/

Zhiqiang Wu[a], Gang Wang[a], Mengwei Zhang[a], Ke Wang[a,*], and Qiang Fu[a,*]

Nucleating agent (NA) species with solubility and self-assembly ability can readily and effectively manipulate the crystalline morphology of semicrystalline polymers through construction of heterogeneous frameworks prior to primary crystallization of basal resins. However, the solubility of NA is difficult to be assessable by current traditional methods. In this study, gradient temperature field (g-T field) was utilized, for the first time, to ascertain the dissolution and self-assembly behaviors of β-NA in the melts of isotactic polypropylene (iPP). The g-T field technique can facilely assess the soluble behavior of β-NA through determining the transformation between several NA frameworks, namely, needle-, flower- and dendrite-like supermolecular structures. Clarifying the soluble behavior of β-NA is of great significance to guide the formation of various crystalline frameworks under the homo-temperature fields and control the resultant crystalline morphology of β-modification iPP. Some interesting findings are summarized as: (1) an in-situ observation under g-T field clearly indicates the sequential occurrence of various nucleation and crystallization events on the same observed window, and approves for the migration of well molten β-NA, (2) the exact correlation between T_f and framework type reveals that an abrupt transformation (over narrow temperature range of 1°C) occurred between needle-like and dendrite-like frameworks, (3) the primary crystallization of iPP is strongly depending on the construction mode of β-NA framework.

1. Introduction

A majority of polymer species are crystallizable, and classified as semicrystalline polymer, because their crystallinities are commonly hard to reach or approach 100%. Obviously, many physical performances of semicrystalline polymer are strongly depending on the crystallization properties, such as crystallinity, crystallization rate, crystal size, crystallographic texture, and crystalline morphology[1-3]. The latter issue exhibits enormous attractions in both of academics and real application fields. A good example is relevant with polyethylene (PE), which has the most-simple chain repeat unit and architecture. Even with an unchanged chemical composition and molecular weight, Young's modulus of PE can be enhanced for three orders as varying its crystalline morphology from spherulite, to oriented lamellae, to shish-kebab, and finally to extended chain cylinder. So a significant self-enhancement effect can be achieved[4], which leads to the application diversity of PE materials. There are several methods frequently used to manipulate crystalline morphology, including chemical synthesis[5], externally applied shearing/flowing fields[6, 7], heterogeneous nucleation [8], etc. Among these methods, the adding of nucleating agent (NA) act as heterogeneous nuclei is considered as the most simple and effective one for facilitating and guiding polymer crystallization.

For a common situation, tiny grains of heterogeneous NA may significantly reduce spherulitic size and increase nucleus density per unit area[9, 10] . More interestingly, some NA species consisted of low-molecular-weight organic compounds offer the opportunity to achieve particular fashions of crystalline morphology. These NAs can partially or completely dissolve in the melts of basal polymers, and self-assemble into special supermolecular structures like microfibrillar network[11], needles[12] and complex aggregates[13], during the subsequent process of melt cooling. These heterogeneous crystalline frameworks with large profile sizes and complicated shapes guide the formations of variety of crystalline morphologies, such as monotectic[12], transcrystallinity[13], shish-kebab[14], lamellae interlock[15], microcrytallinity agglomerate[16]. Kristiansen et al.[17] plotted a binary phase diagrammatic drawing of isotactic polypropylene (iPP)/sorbitol derivatives (DMDBS) blend to declare the scenario of phase transition occurred with decreasing temperature from homogeneous liquid phase to liquid-liquid phase separation, to liquid-solid, and, finally, to solid-solid (crystalline-crystalline) separation. In a wide concentration range of DMDBS, microfibrils will be

[a] College of Polymer Science and Engineering, Sichuan University, State Key Laboratory of Polymer Materials Engineering, Chengdu 610065, People's Republic of China
Tel: 0086-28-85461795, Emails: wkestar@scu.edu.cn (K. W.), qiangfu@scu.edu.cn (Q. F.)

generated prior to iPP crystallization and guide the formation of monotectic phase morphology, which is closely relevant to the optical transmittance of nucleated iPP. Varga et al.[18] systematically ascertained the solubility and nucleation duality of a β-modification NA (β-NA), N,N'-dicyclohexyl-2,6-naphthalenedicarboxamide (NJS), for iPP. By varying the concentration of NA (CN) and final temperature of heating (T_f), NJS can self-organize into various spermolecular structures such as needles, dendrites, microcrystalline structures and flower-like agglomerates. Their study suggested an effective pathway for manipulation of iPP crystalline morphology. Other works[19, 20] utilized a kind of aryl amide-based compound TMB-5 as β-NA of iPP. The formation of TMB-5 microfibrillar entities helps to achieve fine shish-kebab morphology in the injection-molding parts of β-nucleated iPP and, interestingly, results in excellent comprehensive mechanics, i.e., simultaneously toughening and strengthening. The manipulation of crystalline morphology by the soluble behaviour and self-assembly of NA was also referred to other semicrystalline polymers like the most conventional biodegradable species, poly(lactic acid) (PLA), which possesses slow crystallization rate and low crystallinity [21]. Bai et al.[22] demonstrated that a benzenetricarboxylamide derivative (TMC-328) can act as high efficiency NA for PLA. Importantly, through intermolecular hydrogen bonding of the amide groups, TMC-328 is capable of self-organizing into fine microfibrils and, subsequently, guide PLA crystallize into spindle-like or shish-kebab-like morphology. A synergistic effect of shearing/flowing field and TMC-328 microfibrillar template can induce oriented shish-kebab entities in the injection-molded parts and significantly improve the mechanical strength and modulus[23]. In another work of Bai et al.[24], through using hot-compression technique unique lamellae interlock structure of shish-kebab formed in the sheets of PLA/TMC-328, and the gas barrier property was increased surprisingly for 500 times. Most recently, Fan et al.[25] successfully synthesized a new hexanedioic acid dihydrazide-based NA, BHAD, for PLA. Due to its solubility depending on concentration and processing temperature, BHAD can self-assemble into needle-like, furcated-fiber-like, or dendrite-like crystalline frameworks in PLA melts, showing the good ability to control the crystalline morphology of PLA.

In recent years, a kind of rare earth-based β-NA for iPP has attracted extensive attention. This β-NA is a heteronuclear dimetal complex of lanthanum, calcium and some specific ligands with the general formula of $Ca_xLa_{1-x}(LIG1)_m(LIG2)_n$, where x and 1- x are the proportions of Ca^{2+} and La^{3+} ions in the complex, LIG1 and LIG2 are dicarboxylic acid and amide-type ligands, respectively [26]. Since its extremely high efficiency and selectivity for introduction of β-modification iPP[27], the rare earth NA showed a significant potential in industrial and real application fields, and a commercial product with the trade name of WBG-Ⅱ is now available in market. More interestingly, it was clearly demonstrated that WBG-Ⅱ has solubility in iPP melts and can be capable of self-assembly into special supermolecular structures[28], which is of significance to control the crystalline morphology of iPP. Luo et al.[29] utilized WBG-Ⅱ to generate spherulite, transcrystallinity and microcrystallinity agglomerate morphology in the hot-compression molded sheets of iPP, and revealed the underlying correlation between β-crystalline morphology and toughness/ductility. The importance of the rare earth NA seems more and more obvious in literature. It was frequently used as nucleating modifier to manipulate the crystalline morphology and to tailor the crystalline behaviour and physical properties for various PP-based materials, such as iPP[30], PP random copolymer[31, 32], impact PP copolymer[33], and even rubber-toughened PP blend[34].

As mentioned above, the solubility of NA in the melts of basal polymer plays a dominant role on the mode of NA self-assembly, the NA framework type and, consequently, the resultant crystalline morphology, which is strongly depending on the factors of CN, T_f, and thermal history of heating/cooling[35]. So a challenge is proposed as: facilely and accurately assessing the soluble behavior of NA under specific conditions. However, it is difficult to be assessable by current traditional methods. For example, even CN and heating/cooling procedure are fixed, in order to elucidate the dependence of NA solubility on T_f the operation circle of melt-cooling-isothermal-heating-melt should be performed for many times under the homo-temperature field to identify the type of NA framework formed upon different T_fs[28]. Obviously, such method is of troublesome and low efficiency, resulting in the exact correlation between NA soluble behavior and T_f (or CN) is by far rarely reported in literature.

In this work, we utilized the gradient temperature field (g-T field), for the first time, to ascertain the dissolution and self-assembly behaviors of the rare earth β-NA, WBG-Ⅱ, in the melts of iPP. As compared to the homo-temperature field (homo-T field), a tremendous advantage of the g-T field is: the assessment of NA soluble behaviour within certain T_f range could be realized by one-time examination. Since the g-T field can cause different dissolved modes of β-NA in one specimen, various NA frameworks and crystallization events will appear in the same observing window, obeying a certain sequence. The research performed under g-T field might provide useful information, which is relevant to the dependence of β-NA solubility on T_f, to guide the constructions of specific crystalline frameworks in the iPP melts with different WBG-Ⅱ concentrations between 0.025 and 0.5 mass percentage. Thus a diagrammatic drawing could be plotted to demonstrate the tansformation between different kinds of NA framework with taking into account CN and T_f. Finally, the effects of NA crystalline framework on the iPP crystallization behavior and the resultant crystalline morphology were clarified by a combination of polarized light microscopy and differential scanning calorimetry. The results acquired in this study could offer new insights into the designing of crystalline morphology in crystallizable polymers by adding dissoluble NA.

2. Experimental

2.1 Materials and sample preparation

A commercially available isotactic polypropylene (iPP) with Mw = 39.9× 10^4 g/mol and Mw / Mn = 4.6, was purchased from Dushanzi Petroleum Chemical Incorporation (Xinjiang, China). A small amount of antioxidant (Irganox 1010) has been added to the as-received iPP. The rare earth β-NA, trademark as WBG-□, was kindly supplied by Winner Functional Materials Company (Foshan, Guangdong, China).

To realize the uniform dispersion of β-NA, iPP granules and WBG-□ powders were first mixed in a hermetic bag and then melt-mixed into a master-batch containing 5 wt% WBG-□ in a Haake internal mixer (Rheomix 600) with a rotate speed of 90 rpm and a processing temperature of 210 °C for 10min. By adding pure iPP into the master-batch, a series of iPP/β-NA specimens with WBG-□ concentrations as 0.025, 0.05, 0.1, 0.2, 0.3, 0.5 wt%, were prepared under the processing conditions of 90 rpm and 190 °C for 10min. These selected concentrations of β-NA are located within a reasonable range for real applications of WBG-□.

2.2 Polarized light microscopy (PLM)

The investigation of PLM under homo-temperature field was performed by using a Leica DMIP polarized optic microscope equipped with a Linkam THMS 600 hot stage. The slices of specimen were heated to the desired T_fs and held for 5 min, then cooled to the selected crystallization temperatures (135 or 137 °C) for morphological observation, under a cooling rate of 5 °C/min. The photographs of crystalline morphology were acquired with the aid of digital camera. On the other hand, the PLM observation under g-T field was proceeded on an Olympus BX-51 polarized optic microscope equipped with a DP 27 CCD. The temperature gradient was provided by a Linkam GS350 double temperature-controlled hot stage, in which a gap of 2 mm acting as the observation window exists between two individually temperature-controlled planes, and the continuous variation of temperature is realized through this gap. The slices of specimen were melted and held at a preseted g-T field for 5 min, and then the two planes were cooled simultaneously under the same cooling rate of 5 °C/min. The photographs of crystalline morphology were acquired during the non-isothermal process. For all of the PLM investigations, the real temperatures on specimens were calibrated by thermal couple.

2.3 Differential scanning calorimetry (DSC)

The non-isothermal crystallization thermograms of the specimens were recorded by using a Perkin-Elmer pyris- Ⅰ DSC instrument with nitrogen as purge gas and calibrated by indium. The specimen about 5 mg was heated to a desired T_f, holding for 5 min to melt iPP crystals and partially or completely dissolve β-NA, and then was cooled to 50 °C under a cooling rate of 10 °C/min. The crystallization temperature, Tc, could be obtained during the cooling process.

2.4 Tensile mechanical testing

The dumbbell-shaped parts with thickness of 2 mm and width of 4 mm in testing section were prepared on a micro-injection molding equipment (HAAKE MiniJet, Thermo Fisher Scientific). The iPP/WBG-□ granules were melted at various T_fs for 5 min, and injection-molded into the parts with mould temperature of 60 °C and pressure of 800 bar. Tensile mechanical testing was conducted on a universal testing machine (Instron 556) with a 10 kN load cell under a crosshead speed of 50 mm/min.

3. Results and discussion

3.1 Determination of β-NA solubility by using the g-T field

The temperature gradient hot stage is a powerful tool to profoundly ascertained some particular structural/morphological issues sensitive to temperature variation, involved with crystallization of semicrystalline polymer[36], microphase separation of block copolymer[37], phase morphology of polymer blend[38], and construction of surface gradient structure for realizing functionality[39], etc. A specially structural design of hot stage for realizing temperature gradient is presented in Fig. 1(a). Two individual planes (a, b) are temperature-controlled independently, and a gap (c) with width of 2 mm exists between these two planes and acts as observation window. The controllable g-T fields are formed across the gap. For example, as showing in Fig. 1(b), an ideal linear relationship exists between temperature and distance as that: temperature steadily and continuously varied from 212.5 °C to 222.5 °C throughout a distance of 4000 μm, i.e., resulting in temperature gradient of 1 °C/400 μm. The middle zone with width of 2000 μm is corresponding to observation window.

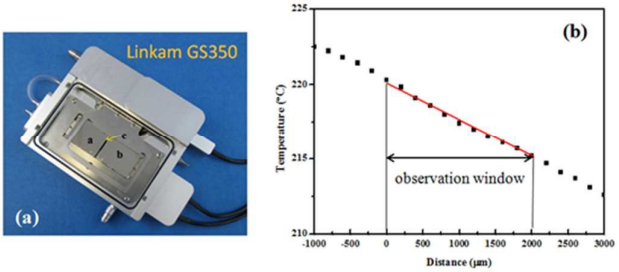

Fig. 1 (a) Digital picture of Linkam GS350 hot stage. (b) A gradient temperature field generated on the observation window of GS350 hot stage

The g-T field presented in Fig. 1(b) was utilized to melt the iPP specimen with 0.1 % β-NA. After holding for 5 min, both of the temperature-controlled planes were cooled under the same cooling rate. The development of crystalline morphology during the cooling process has been followed by PLM, and the corresponding photographs are presented in Fig. 2. As seeing Fig. 2(a), an observing window with width of about 1400 μm is recorded, and the involved T_f range is from 216 to 219 °C. At the initial stage, the PLM photograph is featureless and almost blank. With proceeding the cooling process, the first appearance of crystalline framework is needle-like entity. Numerous needles aggregate at the right side of Fig. 2(b), to generate a specific zone with width of about 500 μm. Subsequently, in Fig. 2(c), the tips of several needles located at

the left boundary of needle zone start to furcated, as indicated by the white arrows. Distinct furcated entities on the tips of needle are also indicated by the white arrows in Fig. 2(d). This framework type is named as flower-like supermolecular structure, because its profile is likes several petals flowering on the end of a stem. Simultaneously, dendritic entities are appreciable as the subjects of the orange arrows. The profiles of dendrite-like framework become more distinct, as indicating by the orange arrows, to result in a dendrite aggregation zone on the left side of Fig. 2(e). In the same photograph, a blank zone without any crystalline entities existed between dendrite-zone and flower-zone is clearly identified by a yellow dash-line rectangle. Despite of the development of β-nucleated crystallization in the β-NA framework zones, as shown in Fig. 2(f), the blank zone keeps unchanged until the appearance of α-nuclei of iPP through a homogeneous nucleation mechanism (the cyan arrows in Fig. 2(g) and (h)). The ultimate crystalline morphology is presented as Fig. 2(i), in which an obvious α-modification zone appears between two β-modification zones that were introduced by flower/needle-like framework and dendrite framework, respectively. So the entire scenario described sequential occurrences of various nucleation and crystallization events in the same iPP/β-NA specimen has been vividly elucidated through Fig. 2.

Moreover, two issues are valuable to be emphasized. (1) The uniform dispersion of β-NA in iPP basal resin has been realized by the two-step melt-mixing procedure including masterbatch and dilution, which can be approved by other figures (Fig. 3 and Fig. S1). Nevertheless, the blank zone without any crystalline entities distinctly exists in Fig. 2(e) and (f), indicating the migration of molten β-NA along the temperature gradient direction. The well-melted β-NA substances possess good mobility and will preferentially migrate to the vicinity of the pre-formed or pre-existed β-NA frameworks through the thermal diffusion behaviour[40,41]. Since many amounts of molten β-NA substances have participated in the self-assembly to formation of flower-like framework, the appearance of the zone absent of β-NA substances is expectable. Moreover, in order to exclude the possibility that the blank zone is arisen from the inhomogeneous dispersion/local aggregation of β-NA, a comparative analysis of nucleation morphology obtained via homo-T field and g-T field is presented in Fig. S1. Numerous microfibrillar-like entities homogeneously exist in the whole observation window after treated by homo-T field. Subsequently, in the same observed window, a distinct blank zone can be seen after experiencing the g-T field treatment. The underlying mechanism of the blank zone is still been exploring in our group. (2) It is well known that the solubility of rare earth β-NA in iPP melt is variable depending on its concentration and processing temperature (e.g., T_f), which plays a dominant role on the self-organization ability and type of crystalline framework[28-30]. The exact correlation between T_f and type of β-NA framework is readily achieved through one-time g-T field examination. In particular, the disappearance of needle-like framework occurs between 217 °C to 218 °C (the red dash line across Fig. 2(a) and (d)), in which the tips of needle furcated into dendrite, indicating that a change in the construction mode of β-NA framework. The transformation from needle-like type to dendrite-like type is corresponding to the soluble behaviour of NA transferred from partially dissoluble to completely dissoluble[18, 25]. The possible procedure of dendrites formation is proposed as that: under the situation of completely dissolved β-NA, microfibrillar entities with very short length appeared at first, then the furcated growth occurred on the two tips of a microfibril, thus a 2D growth mode replaced the 1D growth along the length direction, resulting in dendrite-like crystalline framework. So the crucial T_f regime relevant to dramatic change in β-NA soluble behavior can be facilely assessed by using g-T field technique. Similar to the case of 0.1 % concentration, such T_f regimes were also identified for other CNs, which are of great meaningful to construction of β-NA crystalline framework under traditional homo-temperature field.

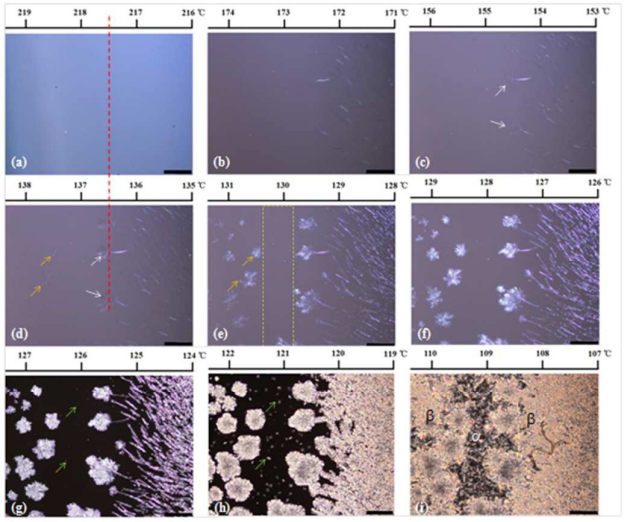

Fig. 2 Development of the crystalline morphology under gradient temperature field (the specimen with 0.1 % β-NA, the scale bar is 200 μm)

3.2 Construction of crystalline frameworks under homo-temperature fields

The specimens with different β-NA concentrations were melted separately at a series of T_fs and cooled to a certain temperature for PLM observation. According to the quality of the photographs acquired, the selected observation temperatures might be not same, 135 or 137 °C, for different conditions. Three compositions of 0.3 %, 0.1 % and 0.05 % are chosen to be representive of high, middle and low concentration, respectively.

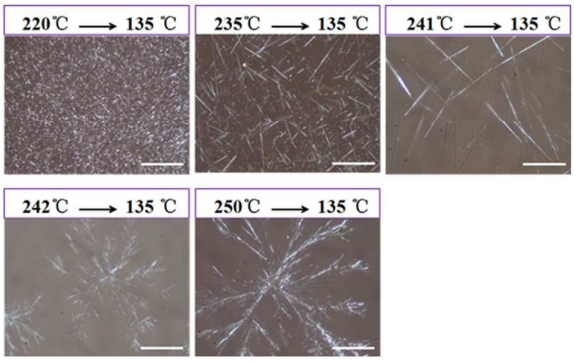

Fig. 3 Morphological photographs of crystalline framework generated in the iPP/WBG-Ⅱ specimen with 0.3 % β-NA (the scale bar is 100 μm)

Some typical morphologies of β-NA framework are shown in Fig. 3 and provided as Supporting Information (Figs. S2, S3), and the T_fs selected in these figures are referring to the g-T field examinations. For the specimen containing 0.3 % WBG-□ (seeing Fig. 3), three types of supermolecular structures are found in sequence of tiny ellipsoids, needles and dendrites as elevating T_f from 220 °C to 250 °C. The raw WBG-□is a kind of irregular block-like crystal, and the diameter and length of a single crystal is about tens of nanometer and less than 1 μm, respectively[28]. Tiny ellipsoidal grains with shape anisotropy reserve the geometrically structural feature of the raw WBG-□, indicating that the solubility of β-NA is very limited at 220 °C. Since the specimen preparation was conducted under a lower molten temperature, 190 °C, WBG-□could exist as a fashion of ellipsoidal grain in the initial specimen before PLM observation. When T_f is high as 241 °C, fine needle-like supermolecular structures with long length (larger than 150 μm) are found. As to the T_f between 220 °C and 241 °C, both of tiny grains and needles coexist in one specimen, indicating that these should be independent affairs. The length and diameter of needle-like framework at 235 °C are obviously smaller than that at 241 °C. This phenomenon implies that the higher T_f is favorable for more fine needle-like construction. In general, the formation mechanism of needle-like framework is due to the increased solubility of β-NA and thus to afford the opportunity for the occurrence of self-assembly behavior. At a higher T_f, such as 250 °C, dendritic framework with extremely large size (occupied the entire observation window) is seen. As to the needle-to-dendrite transition regime determined by g-T field technique, a careful examination was conducted with changing T_f as 1°C-by-1°C, and began at 241 °C. It is surprising that, unlike to the situation of ellipsoid-to-needle, needle-like morphology transferred into dendrite-like morphology is abrupt over an interval of only 1 °C without the so-called coexistence region for these two kinds of crystalline framework. This interesting phenomenon indicates that there are critical T_fs for β-NA completely dissolved, which is 242 °C in the case of 0.3 % WBG-□ concentration.

The morphologies of β-NA framework in the specimen with 0.1 % WBG-Ⅱ are demonstrated as Fig. S2. The morphological features and the rule of construction of β-NA crystalline framework as a function of T_f are almost same to the case of 0.3 % concentration, except for the dendritic entities are more dense and with significantly smaller size. This difference in dendritic morphology is due to the absolute amount of WBG-Ⅱ reduced substantially. In accordance with expectation, the abrupt change from needle to dendrite is also identified, and the critical T_f of entirely dissolvable β-NA is 218 °C at this WBG-Ⅱ concentration, which is well accordance with the result achieved under g-T field (seeing Fig. 2). As to a lower concentration, 0.05 %, the flower-like supermolecular structure appears between needles and dendrites, as shown in Fig. S3. It should be noted that the transformations from needle to flowers, then to dendrites are all over a narrow temperature scope of 1 °C, and the critical T_f for the full solubility of β-NA is determined at 201 °C. Obviously, the more the β-NA amount, the higher the critical T_f is received.

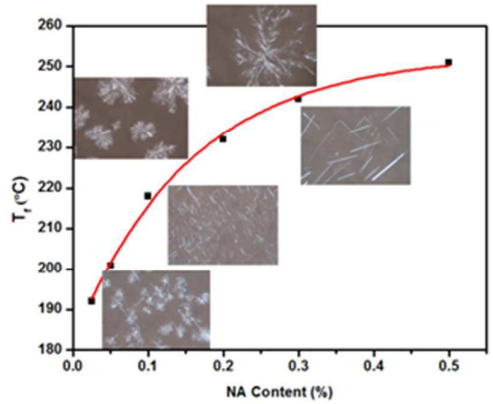

Fig. 4 Transformation of crystalline framework from needles to dendrites depending on T_f and β-NA concentration

By plotting all of the critical T_fs as a function of β-NA concentration, an unambiguous boundary is established in Fig. 4, to clearly demonstrate the transformation behavior from needle-like framework to dendrite-like framework, which is of significance to control the crystalline morphology in iPP/β-NA materials. Although the critical melt temperature for achieving needle-like or dendrite-like framework under certain β-NA concentration can be precisely affirmed from Fig. 4, a question is still arisen. The flower-like framework seems to be the intermediate between needle-like and dendrite-like types. However, this supermolecular structure is merely seen at relatively low CN, e.g., 0.05 %. The reason of this phenomenon can be explained with taking into account the result from Fig. 2. Under g-T field examination, the flower-like frameworks indeed appear at 0.1 % concentration. So the extremely rigorous temperature condition makes this kind of crystalline framework difficult to be found at certain β-NA concentrations, by discretely tuning the melt temperature with an internal of 1 °C.

3.3 Primary crystallization behavior of iPP

In order to assess the effect of β-NA solubility on the primary crystallization behavior of iPP, the T_cs acquired from

the DSC thermograms are plotted as a function of T_f for various β-NA concentrations, as shown in Fig. 5. For the pure iPP, T_c remains constant with the variation of T_f, implying that T_f less influences the crystallization behavior of iPP. As to the specimens with WBG-Ⅱ, for all of the β-NA concentrations ascertained, a twofold tendency is easily appreciable. At the first stage, T_c is sensitive to T_f, and the value of T_c continuously decreases with the elevating of the melt temperature. While at the second stage, T_c is almost independent on T_f, similar to the situation of pure iPP. These two stages are divided by a so-called turn-point. A similar phenomenon was also found by Varga et al.[18] based on the NJS-nucleated iPP specimens. They suggested that the transformation from "sensitive" to "insensitive" might be referred to completely dissolve NJS nucleator. In this study, the exact values of the critical T_f for entirely dissolved β-NA can be acquired from Fig. 4, which are 201, 218, 232, and 242 °C at the concentrations of 0.05, 0.1, 0.2 and 0.3, respectively. While the corresponding T_fs at the turn-points are 200.3, 216.2, 231.4 and 240.2 °C, respectively, as shown in Fig. 5. Considering the difference between DSC and PLM technique, these two groups of value are highly approximate with each other. The turn-points can also declare the occurrence of complete dissolution of β-NA. So the crystallization of iPP is strongly depending on the construction modes of crystalline framework dominated by the β-NA solubility. Under the mode of partially dissolved β-NA, the solubility of β-NA is increased gradually with the elevating of T_f, which needs more and more time to construct needle-like framework, resulting in reduced efficiency for nucleating iPP crystallization. After turning into the completely dissolved mode, the solubility of β-NA is unchanged even T_f is increased, and the time needed for construction of dendritic framework is same for all of T_fs in this temperature regime. So the efficiency for nucleation of iPP does not vary further. Moreover, it should be noted that even a trifold tendency of Tc vs. T_f is identified for the high β-NA concentration of 0.3 %. Except the two stages mentioned above, within a low temperature regime (180 to 220 °C), the variation of Tc is weak with increasing of T_f. This phenomenon is due to the dissolution of β-NA becomes difficult under the situation of high concentration. Since the β-NA substances are almost non-molten within the low temperature regime, it needs T_f higher than 220 °C to induce partial dissolution of WBG-Ⅱ.

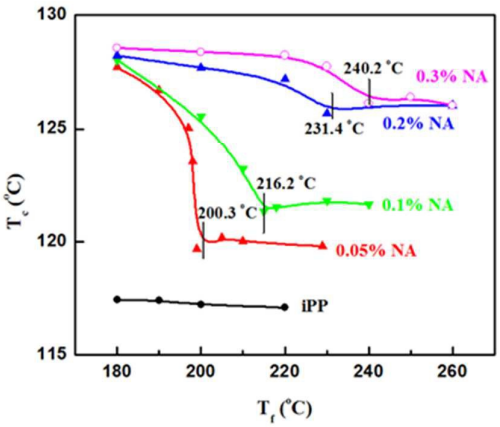

Fig. 5 Correlations between Tc and T_f in the specimens containing different β-NA concentrations

Subsequently, the effects of β-NA framework on the primary crystallization behavior of iPP are elucidated through morphological observation. Typical needle-like crystalline frameworks are found in Fig. 6(a). The surface of β-NA needles can offer sufficient and dense nucleus sites for guiding iPP crystallization on such framework. Since the nucleus density is extremely high, the lamellae of iPP are compelled to grow perpendicular to the length direction of needle entity, which leads to a transcrystallinity morphology (seeing Fig. 6(b)-(d)). Due to uniform dispersion of needle-like entities, it is hard to find the area of iPP homogeneous nucleation. Fig. 7 shows the development of crystalline morphology induced by dendrite-like frameworks. Obviously, the dendrites lead to complex microcrystallinity agglomerates with large size of hundreds of micrometers. In order to form the dendrite-like framework, the coalescence and aggregation levels of β-NA substances are serious, resulting in the non-uniform dispersion of β-NA domains. Some α-nuclei arisen from iPP self-nucleation can be seen during the crystallization process, and the areas of α-modification appear between β-microcrystallinity agglomerates. As to the flower-like frameworks, both of β-transcrystallinity and β-microcrystallinity agglomerate are introduced, meanwhile α-nuclei are generated in certain regions, which finally develop into α-spherulites (seeing Fig. 8).

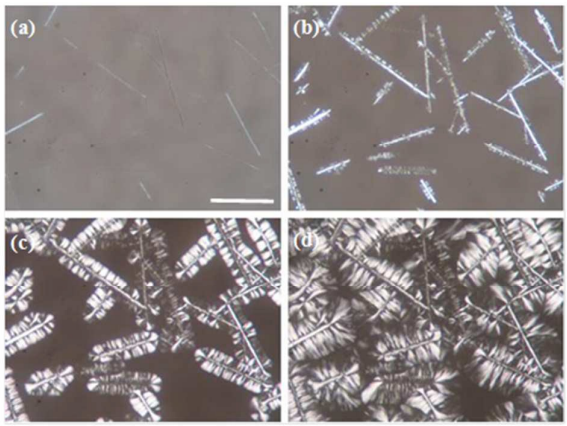

Fig. 6 Evolution of crystalline morphology guided by needle-like frameworks (0.2 % β-NA, Tf = 231 °C, Tc = 135 °C, Cooling rate of 5°C/min): (a) 0 min, (b) 2 min, (c) 6 min and (d) 20 min (the scale bar is 100 μm)

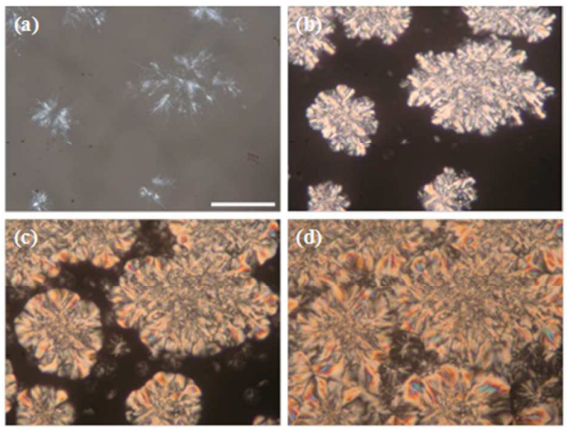

Fig. 7 Evolution of crystalline morphology guided by dendrite-like frameworks (0.2 % β-NA, T_f = 232 °C, Tc = 135 °C, Cooling rate of 5°C/min): (a) during cooling through 137 °C (b) 3 min, (c) 7 min and (d) 20 min (the scale bar is 100 μm

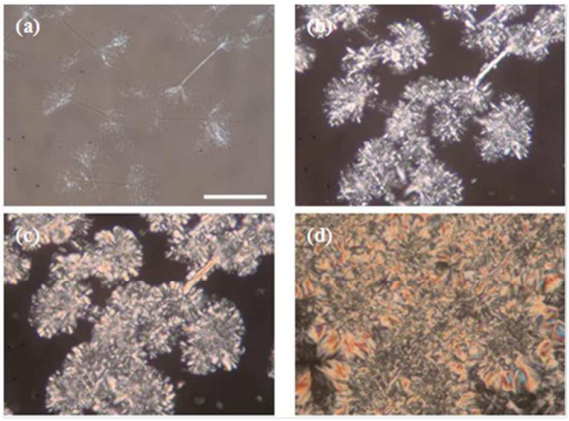

Fig. 8 Evolution of crystalline morphology guided by flower-like frameworks (0.05 % β-NA, T_f = 220 °C, Tc = 135 °C Cooling rate of 5°C/min): (a) during cooling through 137 °C, (b) 1 min, (c) 2 min and (d) 20 min (the scale bar is 100 μm)

3.4 Tensile mechanics

The stress-strain curves for the iPP specimens with 0.1 % β-NA prepared upon different melt temperatures are plotted in Fig. 9. The feature of tensile mechanical behavior is variable with elevating of processing temperature. When the melt temperature is lower than 210 °C, the tensile mechanics is characterized by relatively high strength (up to 42 MPa) but low ductility (less than 100 %). However, as elevating the melt temperature than 220 °C, the character of mechanical behavior is of decreased strength (about 33 MPa) and significantly improved ductility (larger than 450 %). The mechanical behavior observed can be explained reasonably based on a view point of crystalline morphology. In the low temperature regime of 180 to 210 °C, β-NA self-organize into needle-like crystalline framework and induce the transcrystallinity morphology, which is favorable to mechanical strengthening. A dramatic transformation from needle-like to dendrite-like framework may occur at T_f of 218 °C. So the resultant crystalline morphology obtained upon processing temperatures of 220 to 240 °C is a combination of microcrystallinity agglomerates and less α-spherulites, which is benefit to toughness/ductility.

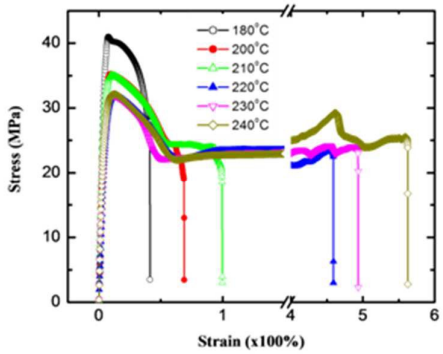

Fig. 9 Stress-strain curves for the specimens with 0.1 % β-NA prepared upon different melt temperatures

Conclusions

The soluble behaviour of β-NA, depending on both factors of CN and T_f, were facilely appreciable by using the g-T field technique. The results obtained via g-T field examination are of great meaningful to guide the construction of β-NA crystalline frameworks by tuning the NA solubility, and thus ascertain the effects of crystalline framework on the primary crystallization behavior and resultant crystalline morphology of iPP. Some new understandings in manipulation of crystalline morphology by adding β-NA with solubility are proposed as: (1) an in-situ observation under g-T field clearly indicates the sequential occurrence of various nucleation and crystallization events on the same observed window, and approves for the migration of well molten β-NA along the direction of temperature gradient. (2) an abrupt transformation (over narrow temperature range of 1°C) occurred between needle-like and dendrite-like frameworks, which is referred to the situation of entirely dissolved β-NA in iPP melt, and (3) the primary crystallization of iPP is strongly depending on the construction mode of β-NA framework. The newly-developed technique of g-T field is desired to, in future, offer more useful information on the formation and evolution of various crystalline morphologies.

Acknowledgements.

Financial supports from NSFC (51421061, 51373108 and 21574088) and the Science & Technology Department of Sichuan Province (2013TD0013) are gratefully appreciated.

References

1. A. El-Hadi, R. Schnabel, E. Straube, G. Müller and S. Henning, *Polymer testing*, 2002, **21**, 665-674.
2. M. Raab, J. Šťudla and J. Kolařík, *European Polymer Journal*, 2004, **40**, 1317-1323.
3. M. Dong, Z. Guo, J. Yu and Z. Su, *Journal of Polymer Science Part B: Polymer Physics*, 2008, **46**, 1725-1733.
4. C. Gao, L. Yu, H. Liu and L. Chen, *Progress in Polymer Science*, 2012, **37**, 767-780.
5. S. Izumikawa, S. Yoshioka, Y. Aso and Y. Takeda, *Journal of Controlled Release*, 1991, **15**, 133-140.
6. C. Zhang, H. Hu, X. Wang, Y. Yao, X. Dong, D. Wang, Z. Wang and C. C. Han, *Polymer*, 2007, **48**, 1105-1115.
7. P.-w. Zhu, J. Tung, A. Phillips and G. Edward, *Macromolecules*, 2006, **39**, 1821-1831.
8. J. Zhang, Q.-J. Ding, N.-L. Zhou, L. Li, Z.-M. Ma and J. Shen, *Journal of Applied Polymer Science*, 2006, **101**, 2437-2444.
9. G.-S. Jang, W.-J. Cho and C.-S. Ha, *Journal of Polymer Science Part B: Polymer Physics*, 2001, **39**, 1001-1016.
10. S. Zhao, Z. Cai and Z. Xin, *Polymer*, 2008, **49**, 2745-2754.
11. J. Lipp, M. Shuster, A. E. Terry and Y. Cohen, *Langmuir*, 2006, **22**, 6398-6402.
12. J. Tang, Y. Wang, H. Liu and L. A. Belfiore, *Polymer*, 2004, **45**, 2081-2091.
13. N. Mohmeyer, H.-W. Schmidt, P. M. Kristiansen and V. Altstädt, *Macromolecules*, 2006, **39**, 5760-5767.
14. P.-w. Zhu and G. Edward, *Macromolecules*, 2004, **37**, 2658-2660.
15. J.-W. Housmans, M. Gahleitner, G. W. M. Peters and H. E. H. Meijer, *Polymer*, 2009, **50**, 2304-2319.
16. C. Marco, M. A. Gómez, G. Ellis and J. M. Arribas, *Journal of Applied Polymer Science*, 2002, **86**, 531-539.
17. M. Kristiansen, M. Werner, T. Tervoort, P. Smith, M. Blomenhofer and H.-W. Schmidt, *Macromolecules*, 2003, **36**, 5150-5156.
18. J. Varga and A. Menyhard, *Macromolecules*, 2007, **40**, 2422-2431.
19. Y.-H. Chen, G.-J. Zhong, Y. Wang, Z.-M. Li and L. Li, *Macromolecules*, 2009, **42**, 4343-4348.
20. Y. Li, X. Wen, M. Nie and Q. Wang, *Journal of Applied Polymer Science*, 2014, **131**.
21. W.-C. Lai, *Soft Matter*, 2011, **7**, 3844-3851.
22. H. Bai, W. Zhang, H. Deng, Q. Zhang and Q. Fu, *Macromolecules*, 2011, **44**, 1233-1237.
23. H. Bai, C. Huang, H. Xiu, Q. Zhang and Q. Fu, *Polymer*, 2014, **55**, 6924-6934.
24. H. Bai, C. Huang, H. Xiu, Q. Zhang, H. Deng, K. Wang, F. Chen and Q. Fu, *Biomacromolecules*, 2014, **15**, 1507-1514.
25. Y. Fan, J. Zhu, S. Yan, X. Chen and J. Yin, *Polymer*, 2015, **67**, 63-71.
26. W. Xiao, P. Wu and J. Feng, *Journal of applied polymer science*, 2008, **108**, 3370-3379.
27. W. Xiao, P. Wu, J. Feng and R. Yao, *Journal of applied polymer science*, 2009, **111**, 1076-1085.
28. F. Luo, K. Wang, N. Ning, C. Geng, H. Deng, F. Chen, Q. Fu, Y. Qian and D. Zheng, *Polymers for Advanced Technologies*, 2011, **22**, 2044-2054.
29. F. Luo, C. Geng, K. Wang, H. Deng, F. Chen, Q. Fu and B. Na, *Macromolecules*, 2009, **42**, 9325-9331.
30. C. Zhang, B. Wang, J. Yang, D. Ding, X. Yan, G. Zheng, K. Dai, C. Liu and Z. Guo, *Polymer*, 2015, **60**, 40-49.
31. F. Luo, Y. Zhu, K. Wang, H. Deng, F. Chen, Q. Zhang and Q. Fu, *Polymer*, 2012, **53**, 4861-4870.
32. F. Luo, J. Wang, H. Bai, K. Wang, H. Deng, Q. Zhang, F. Chen, Q. Fu and B. Na, *Materials Science and Engineering: A*, 2011, **528**, 7052-7059.
33. F. Luo, C. Xu, K. Wang, H. Deng, F. Chen and Q. Fu, *Polymer*, 2012, **53**, 1783-1790.
34. Y. Zhu, Y. Zhao, S. Deng, Q. Zhang and Q. Fu, *RSC Advances*, 2015, **5**, 62797-62804.
35. M. Dong, Z. Guo, Z. Su and J. Yu, *Journal of applied polymer science*, 2011, **119**, 1374-1382.
36. A. Toda, K. Taguchi and H. Kajioka, *Macromolecules*, 2011, **45**, 852-861.
37. G. Singh, K. G. Yager, B. Berry, H.-C. Kim and A. Karim, *ACS nano*, 2012, **6**, 10335-10342.
38. H. Jiang, N. Dou, G. Fan, X. Zhang and Z. Yang, *Polymer*, 2014, **55**, 2271-2278.
39. J. Jang and J. Bae, *Advanced Functional Materials*, 2005, **15**, 1877-1882.
40. K. Taguchi, H. Miyaji, K. Izumi, A. Hoshino, Y. Miyamoto and R. Kokawa, *Polymer*, 2001, **42**, 7443-7447.
41. A. McPherson, A. J. Malkin, Y. G. Kuznetsov, S. Koszelak, M. Wells, G. Jenkins, J. Howard and G. Lawson, *Journal of crystal growth*, 1999, **196**, 572-586.